Ceramics International xxx (xxxx) xxx

Contents lists available at ScienceDirect

Ceramics International

journal homepage: www.elsevier.com/locate/ceramint

Stable water-based luminescent suspensions of Eu^{3+}:YPO_4 nanophosphors in sodium alginate medium: Sustainable inks for potential anticounterfeiting applications

Enrico Paradisi [a], Cecilia Mortalò [b,*], Fernanda Andreola [a], Valentina Zin [b], Raffaella Capelli [a,c], Luca Pasquali [a,c,d], Silvia Maria Deambrosis [b], Enrico Miorin [b], Cristina Leonelli [a]

[a] Department of Engineering "Enzo Ferrari" (DIEF), University of Modena and Reggio Emilia, Via P. Vivarelli 10, Modena, 41125, Italy
[b] Institute of Condensed Matter Chemistry and Technologies for Energy (ICMATE), National Research Council of Italy (CNR), Corso Stati Uniti 4, Padova, 35127, Italy
[c] Department of Physics, University of Johannesburg, P.O. Box 524, Auckland Park, 2006, Johannesburg, South Africa
[d] CNR-Istituto Officina dei Materiali (IOM), Strada Statale 14, Km. 163.5 in AREA Science Park, Basovizza, 34149, Trieste, Italy

ARTICLE INFO

Handling Editor: P. Vincenzini

Keywords:
Eu^{3+}:YPO_4 nanophosphors
Sodium alginate-based inks
Rheology
Stability
Luminescence
Stabilization effect

ABSTRACT

The development of sustainable luminescent inks is attracting increasing attention for applications in security printing, bio-imaging, and visualization technologies. Rare-earth-doped YPO_4 nanophosphors are particularly promising due to their high efficiency, chemical stability, and well-defined emission features. In this work, we present a simple and eco-friendly strategy to formulate fully water-based luminescent inks by combining Eu^{3+}:YPO_4 (5 mol% Eu^{3+}) nanophosphors, synthesized via a microwave-assisted method, with sodium alginate (SA) as a dispersant and rheology modifier. Different grades of SA were investigated to identify the conditions that optimize both dispersion stability and optical performance. Suspensions containing 2 wt% SA and a Eu^{3+}:YPO_4/SA ratio of 1:10 (w/w) exhibited excellent colloidal stability, shear-thinning behavior, and anti-thixotropic properties. ζ-potential and photoluminescence analyses confirmed strong interactions between SA chains and Eu^{3+}:YPO_4 nanoparticles, enabling long-term stability while preserving the characteristic emission of the phosphor. Notably, the SA matrix contributed to enhanced luminescence in the 350–400 nm range, resulting in a dual-emission response from both polymer and nanophosphor. These findings provide a clear proof-of-concept for cost-effective, solvent-free luminescent inks based on environmentally friendly components, highlighting their potential for future integration in anti-counterfeiting and security printing applications.

1. Introduction

Despite the increasing use of information technology to protect data, physical media such as paper or plastic cards are still of primary importance for ensuring the validity of money and documents. The study of new anti-counterfeiting methods for encrypting information on physical media is therefore a top priority to protect and authenticate genuine products. [1–3]. Several anti-counterfeiting technologies have been developed, including watermarks, bar codes, hologram technology, thermal imaging, radio frequency identification, laser coding and fluorescence detection [3–7]. However, many of these approaches are complicated and/or expensive, limiting their practical application.

Conversely, luminescent anti-counterfeiting inks are inexpensive, easy to apply and attractive because they are easily authenticated but difficult to copy [1–3,8]. When exposed to UV radiation, luminescent materials emit light at specific wavelengths, generating unique pattern that can be used for authentication [9]. For these applications, luminescent inks must have high thermal, chemical and photostability, intense luminescence, good adhesion to substrates, suitable viscosity, homogeneous dispersions, and low cost. Dispersants such as polymethyl methacrylate (PMMA), polyvinyl alcohol (PVA), sodium hexametaphosphate and polyvinyl chloride (PVC) have been employed [3]. Various luminescent materials - including carbon/silicon quantum dots [3,10,11], organic dyes [12], metal-organic frameworks [3,13], and rare-earth doped nanomaterials [3,14,15] have been investigated for security applications.

* Corresponding author.
E-mail address: cecilia.mortalo@cnr.it (C. Mortalò).

https://doi.org/10.1016/j.ceramint.2025.10.092
Received 4 July 2025; Received in revised form 1 October 2025; Accepted 6 October 2025
Available online 9 October 2025

Among these, RE^{3+}-doped YPO_4 phosphors are especially promising thanks to their bright and long-lasting luminescence, chemical and thermal stability, especially in their water-free crystal structures, i.e., the tetragonal *Xenotyme-Y* and monoclinic *Monazite* phases [16]. They are widely studied in plasma displays [17], biological labelling [18], imaging [19], fingerprinting [20] and dosimetry [21]. Furthermore, some works report their use also in anti-counterfeiting inks [22–25]. For instance, Zhou et al. dispersed hydrated $(Y_{0.95}Eu_{0.05})PO_4{\cdot}nH_2O$ and anhydrous $(Y_{0.95}Eu_{0.05})PO_4$ particles in PVA medium and obtained films showing strong red luminescence under UV irradiation [25]. Ningthoujam et al. observed the clearly visible colours of YPO_4:Er^{3+}-Yb^{3+} nanophosphors dispersed in methanol and acetone under 980 nm NIR light excitation [22]. Saladino and co-workers obtained long-term stable Eu^{3+}:YPO_4 suspensions in PVA-ethanol/water mixtures [23]. More recently, Kumar et al. developed La/YPO_4:Eu^{3+} nanocomposites for both inks in a polyvinyl chloride PVC gold medium and an aqueous polyvinyl alcohol (PVA) matrix, showing a red-orange colour when irradiated with a short-wave UV lamp (254 nm) and an atomic line (394 nm) [20]. Despite these promising results, most reported formulations still rely on organic solvents or synthetic additives, raising environmental and safety concerns [20,23,26]. Fully water-based, cost-effective inks obtained through simple routes remain rare, as most current systems incorporate polymers such as polyvinylpyrrolidone (PVP), PVA, Polyurethane (PU), or others [27–31]. Only a few examples of truly additive-free, water-based inks have been reported [32–35], underscoring the need for more sustainable alternatives. In this context, our work explores a straightforward strategy based on Eu^{3+}:YPO_4 nanophosphors and sodium alginate to design eco-friendly luminescent inks for potential anti-counterfeiting applications.

Sodium alginate is a biodegradable, water-compatible polysaccharide obtained from brown seaweed [36]. A distinctive feature of SA is its versatility in forming nanocomposites with inorganic nanopowders and other bio-based polymers [37–41]. Its structure, composed of guluronate (G) and mannuronate (M) residues arranged in homopolymeric and alternating blocks, bears carboxylate groups that strongly influence viscosity and gelation behaviour [42]. The G/M ratio, block distribution, and molecular weight are key parameters determining the rheological properties of SA solutions [36,43]. Thanks to the wide range of commercially available grades, SA offers remarkable flexibility in tuning viscosity, from very low to highly viscous solutions, simply by adjusting its type and concentration [44]. These features, combined with its natural origin and biocompatibility, make SA a particularly promising component for the formulation of eco-friendly, tuneable anti-counterfeiting inks.

Several studies demonstrated the potential of Sodium Alginate (SA) in formulation of luminescent inks [9,33,34,45–48]. For example, Xie [33] and Guo [34] prepared SA-based inks containing silicon nanoparticles that emit blue, green or red colours when irradiated with UV light; Cruz et al. [9] developed Europium complex inks using SA as the binder; Mogharbel et al. [45] prepared security inks based on SA hydrogels with natural pigments; Hossan and Al Nami [46] exploited SA with long-persistent phosphors; Das and Maity [47] developed multicolour and UV-responsive SA inks for use on rewritable paper; Wang et al. [48] reported afterglow systems containing SA and aromatic carboxylic acids. These studies demonstrate the potential of RE^{3+}-doped YPO_4 as an efficient luminescent phosphor and the versatility of SA in various ink applications, suggesting promising applications in eco-friendly anti-counterfeiting inks. Combining the low toxicity of RE^{3+}-doped YPO_4 with the natural abundance and biocompatibility of SA would provide a cost-effective and environmentally sustainable method of producing water-based luminescent inks. However, to the best of our knowledge, no reports in the literature have yet described anti-counterfeiting luminescent inks that integrate SA with RE^{3+}-doped YPO_4 as the phosphor.

Recently, we optimized a MW-assisted hydrothermal process for preparing Eu^{3+}:YPO_4 nanopowders under neutral aqueous conditions without using organic additives [49,50]. Indeed, microwave (MW) irradiation is well-known to promote phase transformation and stabilization in materials [51,52], as well as enhancing processes carried out under vacuum [53] or in the solid state [54]. In our case, MW-assisted heating significantly reduced reaction times and yielded nanoparticles with uniform size and morphology. Furthermore, by adjusting the synthesis temperature, we obtained nanopowders with tuneable morphology and photoluminescence properties, enabling their optimization for specific applications [49,50].

The aim of this work was to develop eco-friendly, luminescent inks for potential anti-counterfeiting purposes. To this end, the dispersion behaviour of Eu^{3+}:YPO_4 nanophosphors (5 mol% Eu^{3+}) in aqueous media using sodium alginate as a dispersing agent was investigated for the first time. Thanks to its polyanionic character and the presence of carboxylate and hydroxyl groups, SA was expected to interact with the nanophosphor surface, thereby enhancing colloidal stability and modulating photoluminescence, both of which are crucial for ink performance. The Eu^{3+}:YPO_4 powders were synthesized *via* a microwave-assisted hydrothermal route, while different grades and viscosities of SA were tested. SA suspensions were systematically studied through rheology, ζ-potential, and photoluminescence (PL) spectroscopy to correlate dispersion behaviour with optical response and long-term stability.

2. Experimental

2.1. Materials

$Y(NO_3)_3 \times 6H_2O$ (99.8 %), $Eu(NO_3)_3 \times 5H_2O$ (99.9 %), and KH_2PO_4 (≥98.0 %), were purchased from Sigma-Aldrich (part of Merck KGaA, Darmstadt, DE) and used without further purification. The four grades of sodium alginate were used without further purification.

- SA-VLV: Sodium Alginate Very Low Viscosity (Thermo Fisher Scientific, Waltham, MA, USA), Product number A18565, Lot. 10242904, Viscosity 9 mPas (1 wt% aq. solution, 20 °C);
- SA-LV (1): Sodium Alginate Low Viscosity (Thermo Fisher Scientific, Waltham, MA, USA), Product number B25266, Lot. 10241968, Viscosity 37 mPas (1 wt% aq. solution, 20 °C);
- SA-LV (2): Sodium Alginate Low Viscosity (MP Biomedicals, Irvine (CA), USA, >98 %) Viscosity <300 mPa s (1 wt% aq. solution, 20 °C);
- SA-E401: Sodium Alginate E 401 (FarmaLabor, Canosa di Puglia (Bt), IT, >90 %) at High Viscosity, food grade (food additive E401), viscosity 500–650 mPas (1 wt% aq. solution, 20 °C), manuronic and guluronic acids, ratio: 1,8-2,2.

Distilled water was used for all the preparations in every operation.

2.2. Preparation of/Eu^{3+}:YPO_4 powders

Eu^{3+}:YPO_4 (5 % mol of Eu) nanopowders were prepared by a MW-assisted hydrothermal process as described in Ref. [49]. The synthesis was performed at 200 °C for 20 min, then the powders were washed with distilled water and recovered by centrifugation. The final white product was obtained after drying at 70 °C overnight.

2.3. Preparation of SA solutions and SA/Eu^{3+}:YPO_4 suspensions

Sodium alginate solutions of 1 wt% and 2 wt% were prepared by the following procedure. SA powders (0.5 g for the 1 wt% solutions and 1 g for the 2 wt% solutions) were dissolved in 50 mL of distilled water and the solutions were stirred at room temperature for 48 h. The luminescent inks were then formulated by incorporating Eu^{3+}:YPO_4 nanopowders into the 2 wt% SA solutions, ensuring a constant Eu^{3+}:YPO_4/SA ratio of 1:10. The suspensions were then stirred for a further 24 h.

2.4. Characterization

A Philips X'Pert PRO diffractometer (now part of Malvern PANAlytical, Malvern, UK) equipped with a fast detector (X'Celerator) was used for the *XRD investigations*. The measurement was performed at room temperature using Cu-kα radiation (λ = 1.5405 Å) and at 40 kV and 40 mA in the range 5–90° 2θ with a step of 0.008° and a time for step of 5 s. Phase identification was performed using X'pert HighScore Plus® software.

TEM studies were carried out by a high-resolution scanning/transmission electron microscope (S/TEM) (Thermo Scientific™ Talos™ F200S) equipped with energy dispersive X-ray spectroscopy (EDS) and operating at 200 kV acceleration voltage. Well-dispersed nanoparticles were obtained by sonication of the water (distilled water, Millipore, Milli-Q® IQ 7000) suspensions for 15 min. The specimens were then prepared by immersing 200 mesh copper microscope grids coated with carbon in the sonicated suspension. Finally, the samples were dried and analysed directly. The mean dimensions and particle size distributions were determined by measuring at least 350 individual particles in the TEM micrographs using ImageJ software (version 1.53t). These distributions were then fitted with normal or lognormal functions using the Origin® program to assess which of the two-fit best, and the best fits are shown in the figures reported in the SI.

Rheological tests were carried out using a MCR102e rotational rheometer (Anton Paar, Austria). The shear rheological properties (flow curve and shear viscosity curve) were measured with a cone/plate CP25-1 (D = 25 mm; angle 1°) sensor (gap fixed 50 μm). A Peltier plate temperature device was used both to obtain accurate T control at 25.00 ± 0.01 °C and to avoid solvent evaporation. The suspensions were introduced on the cone/plate measuring geometry and rest 1 min to eliminate the residual shear story. The two-step cycle consists of a shear rate increase from 0 s^{-1} to 1000 s^{-1} followed by a shear rate decrease from 1000 s^{-1} to 0 s^{-1}. This cycle allowed us to qualitatively assess the time dependence according to the type of hysteresis created by the loop [55]. The samples were also tested after 30 days to check their stability over time using the same rheological method.

ζ-potential was evaluated by using a Malvern Zetasizer ZS Nano instrument (Malvern Panalytical, Malvern, UK). 1 ml of the prepared suspensions was introduced in a 20 ml volumetric flask, which was then filled with distilled water for the rest of the volume. The concentration of dilute samples is approx. 0.0001 g/ml, which is claimed optimal to avoid topological interactions (i.e., overlapping or entanglements) eventually occurring in the solutions [56]. 1 ml of such diluted solution was then transferred in a DTS1070 clear disposable Z cell provided by the same supplier for analyses. The parameters for the measurements were:

- Material: polystyrene latex (R.I.: 1.590, Absorption 0.010);
- Dispersant: water (Viscosity: 0.8872 cP, R.I.: 1.330, Dielectric Constant: 78.5);
- Temperature: 25 °C;
- Model: Smoluchowski;
- Analysis mode: auto mode;
- Equilibration time: 120 s;
- Zeta runs: automatic (generally 12–15);
- Measurement position: 2 mm;
- Attenuator: 6–10.

Three measurements were carried out for each sample and then the average value was calculated. This average value is the one reported along this paper for each sample.

PL measurements were carried out on 2 wt% SA solutions and Eu^{3+}:YPO_4/SA suspensions using a CUV Cuvette Holder completely shielded from the ambient light interfaced via fiber optic to a L280A high intensity LED Ocean Optics laser diode with emission at 280 nm wavelength and to a QEProFL Ocean Optics spectrometer. Photoluminescence has been collected at an angle of 90° with respect to the incident laser beam.

3. Results and discussion

3.1. Chemical and morphological characterizations

The crystalline phases present in the as-prepared nanopowders were examined. In Fig. 1 the XRPD pattern of the synthesized Eu^{3+}:YPO_4 (5 % mol of Eu) powders is shown. Powders with a single-phase *Xenotime-(Y)* tetragonal structure with space group $I4_1/amd$ (according to JCPDS: 00-011-0254), corresponding to anhydrous yttrium phosphate (V), is obtained after 20 min of MW-assisted heating at 200 °C, in good accordance with our previous results [49] and with what is reported in literature [57] (Fig. 1). No other secondary phases are detected. Similar results were also reported by Armetta et al. [58], who prepared Eu-doped YPO_4 nanopowders with a tetragonal structure at the same temperature by means of a conventional hydrothermal method. Peak broadening, typical of nanosized crystals, can be noticed in the entire 2θ range.

Since also the powder morphology is as important as the photoluminescence properties in counterfeit inks we investigated the Eu^{3+}:YPO_4 (5 mol% of Eu^{3+}) nanopowders for morphology and dimension of primary crystals by TEM observation at different magnifications (representative micrographs are shown in Fig. 2(a–d)).

Similar to what obtained in our previous work [49], TEM analysis reveals that the nanopowders are composed of single crystals with a mixed morphology consisting mainly of elongated nanoparticles, although some square or irregular ones are also observed. Moreover, the HR-TEM micrograph in Fig. 2(d) shows a well-resolved interplanar spacing of ≈3.5 Å, ascribable to the (200) lattice plane of the *Xenotime-(Y)* tetragonal structure (JCPDS 00-011-0254), in agreement with results obtained by the XRD analysis. The high crystallinity of the particles is corroborated by the sharp ring-type selected area electron diffraction (SAED) pattern shown in Fig. 2(e), which exhibits well-resolved sharp ring-type lines. The elemental EDS maps and Eu and Y elemental profiles are displayed in Fig. S1 (b-f) and (g) of the Supporting Information file, respectively. The EDS spectrum of Eu^{3+}:YPO_4 nanopowders is shown in Fig. S1(h) and quantitative EDS analysis of the sample is reported in Table S1. As evident, only Eu, Y, P and O elements are detected (C and Cu, being the constituents of the sample holder grid) and are homogeneously distributed in the grains. Furthermore, the analysis demonstrates the presence of Eu^{3+} ions, which are well dispersed within the YPO_4 crystalline structure. This finding serves to confirm the efficacy of the doping process and to exclude any potential

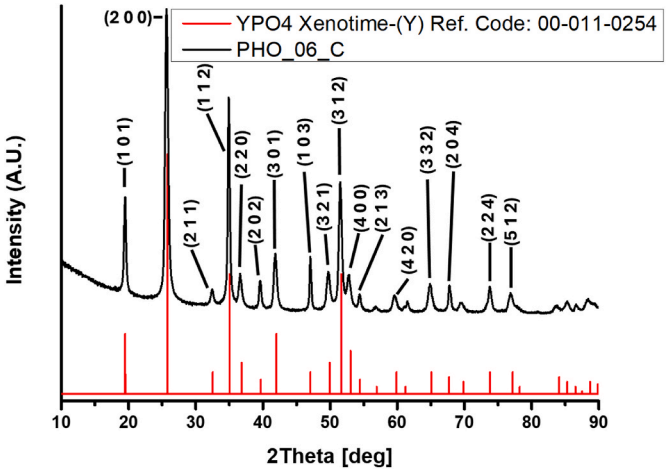

Fig. 1. XRD pattern of Eu^{3+}:YPO_4 (5 mol.% of Eu^{3+}) nanopowders and relevant reflection planes labelled with appropriate Miller indices according to JCPDS: 00-011-0254.

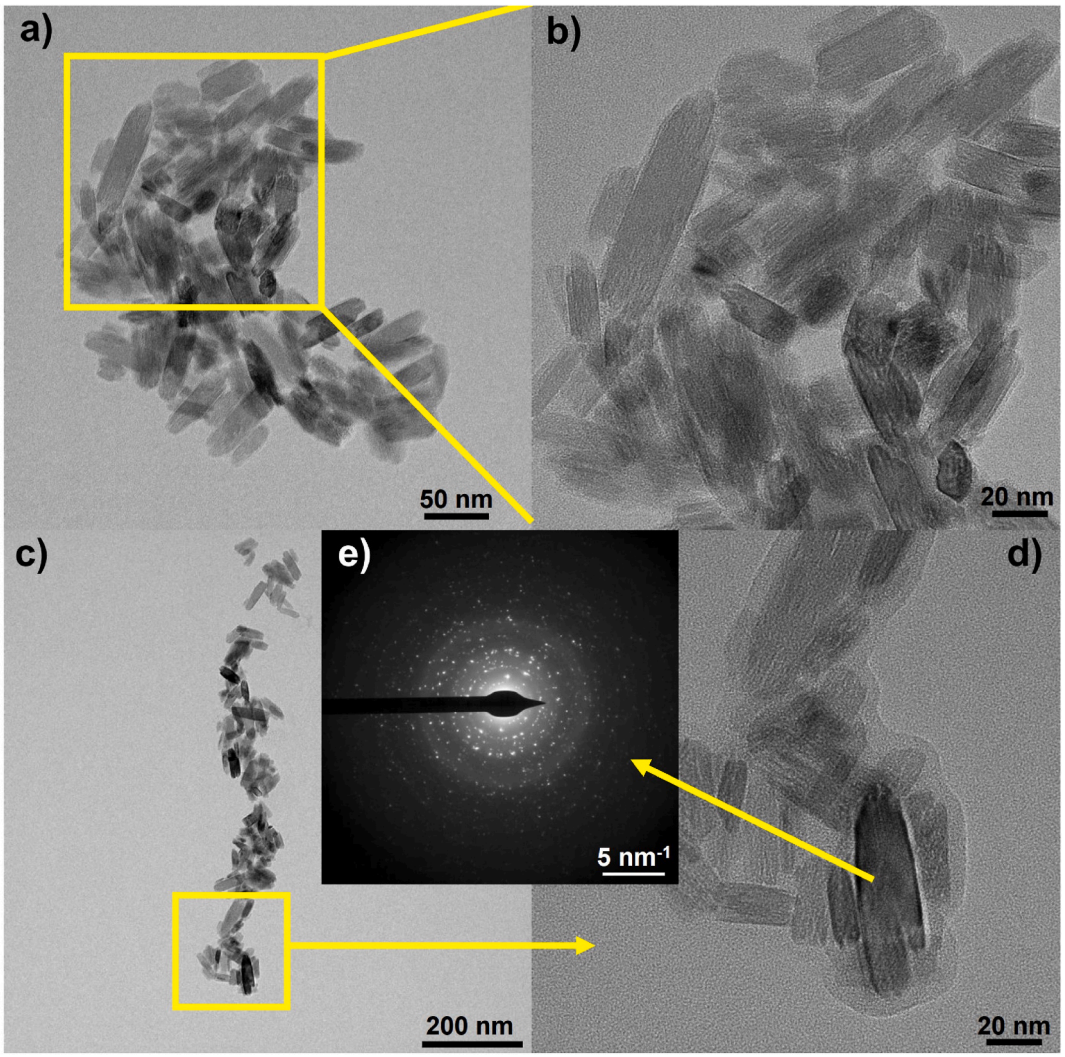

Fig. 2. (a–d) TEM micrographs of Eu^{3+}:YPO_4 nanopowders at different magnification. **(e)**: selected area electron diffraction (SAED) pattern on area shown in Fig. 2(d).

segregation of the dopant. As illustrated in Table S2 and Fig. S2, the mean values and the particle size distributions in both directions, i.e. length and thickness, were calculated by TEM micrographs. Furthermore, the aspect ratio (ratio between length and width) was calculated. The analysis revealed that both length and width exhibited right-skewed lognormal distributions, with a mean particle length of 44 nm and a mean particle width of 16 nm. The majority of the particles demonstrated lengths ranging from 15 to 75 nm and widths from 5 to 25 nm. This finding suggests a slight preponderance of larger particles over smaller particles. Conversely, the ratio L/W exhibited a left-skewed distribution (Pearson IV equation fitted best), with an average L/W of approximately 3 and the majority of nanoparticles displaying L/W values between 1.5 and 4. This finding suggests a marginal predominance of short and wide nanoparticles over long and narrow ones.

As demonstrated in our previous works [49,50], this represents an intermediate situation within a trend that leads the shape of nanoparticles to become longer and narrower, starting from short and wide aggregates of smaller nanosticks, which occur as a result of an increase in both the synthesis temperature and time. The selection of this intermediate state as the focal point of the present study on inks was driven by the necessity to establish a reference point for rheological measurements and ancillary studies. This reference point could then be utilised for comparison with the results of future studies, which will focus on the most "extreme" morphologies.

3.2. Rheological behaviour

Fluids, suspensions included, may be investigated in terms of rheological behaviour. In the context of Newtonian fluids, the shear stress (τ) is directly proportional to the shear rate ($\dot{\gamma}$) or strain rate (γ), as elucidated by Newton's equation (1) [59]. The ratio between shear stress and shear rate is defined as apparent viscosity (η).

$$\tau = \eta^* \dot{\gamma} \qquad \text{Equation 1}$$

For non-Newtonian fluids, the apparent viscosity is not constant, and in the specific case of a pseudoplastic or shear-thinning behaviour, the apparent viscosity decreases with increased stress. This can be described by the Ostwald model (power law), as supported by other studies [60].

$$\tau = K \dot{\gamma}^n \qquad \text{Equation 2}$$

where τ is the shear stress (Pa), K is the consistency index (Pa·s^n), γ is the shear rate s^{-1} and n is flow behaviour index.

The SA solutions were found to be non-Newtonian fluids, i.e. exhibiting variable viscosity according to the applied force or flow rate, and thus displaying shear-thinning rheological behaviour. It is very important to measure rheological properties for every batch every time, since the rheological features can vary depending on the specific SA batch [61]. The present study analysed the rheological behaviour of four different SA polymer solutions at two concentrations (1 and 2 wt%) in

order to ascertain the most effective method of preparing suspensions with Eu^{3+}:YPO_4 nanopowders. The rheology measurements were taken on freshly prepared solutions and after 30 days in order to evaluate solutions' stability.

The results of the apparent viscosities and flow indexes for all solutions and suspensions considered in this study are summarized in Table 1. The Ostwald model was applied to the SA solutions prepared at 1 wt%, and it was observed that the SA solutions LV (1), LV (2) and VLV show flow index, *n*, values between 0.94 and 1.03, indicating that the effect of SA on solution viscosity is negligible and that the rheological behaviour is mainly due to the water solvent. Conversely, SA-E401 exhibited a pronounced shear-thinning behaviour with n = 0.67. The effect of SA concentration on rheological parameters was therefore investigated by increasing the SA concentration in solutions to 2 wt%. The resulting solutions exhibited elevated viscosity values and a decline in the flow index, indicative of a pronounced shear-thinning tendency. This behaviour is considered favourable in the preparation of inks, and so a 2 wt% concentration was selected for further data analysis.

The viscosities *vs* shear rate of 2 wt% SA aqueous solutions are plotted in Fig. 3: similar to what observed by Rodriguez Rivero et al. all solutions show a shear-thinning behaviour [62]. This phenomenon has been attributed to the deformation of the polymer coils and their subsequent alignment in the direction of flow, thereby providing a reduced resistance to flow as the applied shear rate increases. This is a well-documented occurrence within the field of polymer science, particularly in instances where polymeric molecules are present in a solvent comprising smaller molecules, such as SA solutions at low concentrations [63]. A thorough analysis of the viscosity values across all the curves (Fig. 3) and at the maximum shear rate applied for each SA grade (Table 1) reveals a clear trend of increasing viscosity in a specific order: **SA-VLV, SA-LV (1), SA-LV (2), SA-E401**. This observation lends strong evidence to support the hypothesis that the rheological parameters are contingent on the type and concentration of SA employed. Subsequent to a 30-day period, the same samples were tested to ascertain their stability over time using the same rheological method. As demonstrated in Fig. 3, the SA solutions exhibited a consistent shear-thinning behaviour, with only a marginal decline in viscosity values (with the exception of **SA-LV (1)**, as indicated in Table 1). These data suggest a good dispersion of the polymeric matrix without substantial settling phenomenon during the storage period. It is noteworthy that the solutions were not subjected to stirring during the 30-day storage period.

The time-dependence evaluation, as conducted through the analysis of the hysteresis loop into flow curves (see Fig. 4), indicates that the systems demonstrate a slight anti-thixotropic behaviour, a finding that aligns with the observations reported by Belalia et al. [61].

Table 1
apparent viscosities and flow indices of all samples, both as-prepared and after 30 days.

Sample	Apparent Viscosity at 1000 s^{-1} (mPa.s)[a]		Flow index *n*	
	As prepared	After 30 days	As prepared	After 30 days
SA-VLV 1 wt%	6.08	/	1.03	/
SA-VLV 2 wt%	16.46	16.45	0.891	0.804
SA-LV (1) 1 wt%	18.79	/	0.940	/
SA-LV (1) 2 wt%	74.08	75.07	0.930	0.941
SA-LV (2) 1 wt%	37.30	/	0.948	/
SA-LV (2) 2 wt%	153.22	145.70	0.778	0.851
SA-LV (2) 2 wt% + Eu^{3+}:YPO_4	159.74	134.85	0.766	0.872
SA-E401 1 wt%	69.84	/	0.671	/
SA-E401 2 wt%	243.67	243.57	0.627	0.647
SA-E401 2 wt% + Eu^{3+}:YPO_4	260.00	235.89	0.583	0.619

[a] The measured data of viscosity are affected by an absolute error of 1 %.

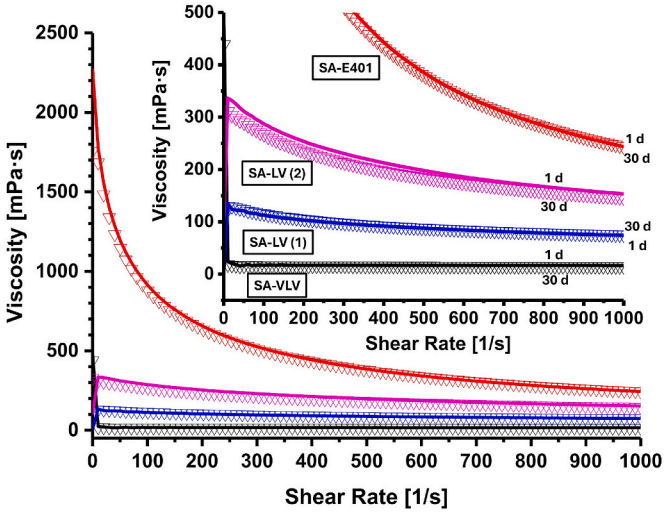

Fig. 3. Viscosities *vs* Shear rate for all as-prepared (1d) SA solutions and after 30 days (30d).

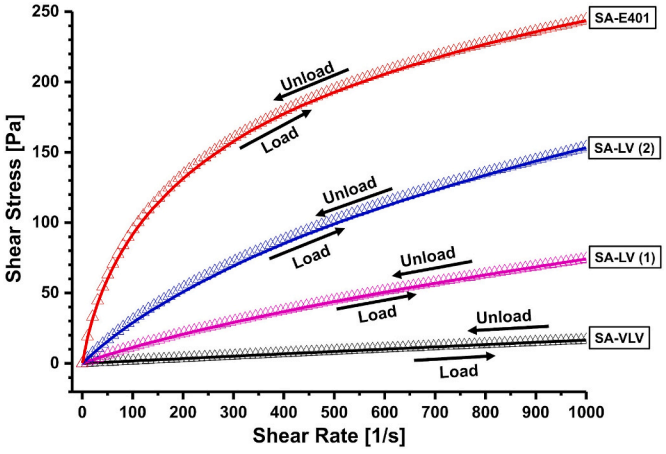

Fig. 4. Flow curves (shear stress *vs* shear rate) for all as-prepared SA solutions.

Consequently, viscosities exhibit a modest increase in the return curve (unload) upon decreasing the shear rate after its initial increase, suggesting a reorganization of polymer chains into slightly more robust structures.

3.2.1. *Effect of phosphors*

In view of the elevated viscosity values exhibited by the solutions **SA-LV (2)** and **SA-E401** at 2 wt%, they were considered optimal for their utilisation in anticounterfeiting inks. These two solutions were thus further added with Eu^{3+}:YPO_4 nanopowders and the so-obtained suspensions rheologically tested, as before, both fresh and after 30 days. The analysis of the flow curves by the Ostwald model revealed that the addition of Eu^{3+}:YPO_4 nanopowders to SA solutions did not influence their rheological behaviour, as evidenced by the observation of shear-thinning behaviour in both cases (see Table 1 and Fig. 5). With regard to the viscosity values interpolated at a maximum shear rate (1000 s^{-1}), a modest increase is observed for **SA-LV (2)** (4 %) and **SA-E401** (7 %), thereby confirming that rheological parameters are influenced by the contribution of the disperse phase. The underlying factors contributing to this phenomenon may include the volume fraction of particles, the morphology of the particles, the inter-particle interactions, and the spatial arrangement of the particles [59].

Comparing the stability values after 30 days (when the suspensions were kept at rest) it was noted that the flow index increased and the

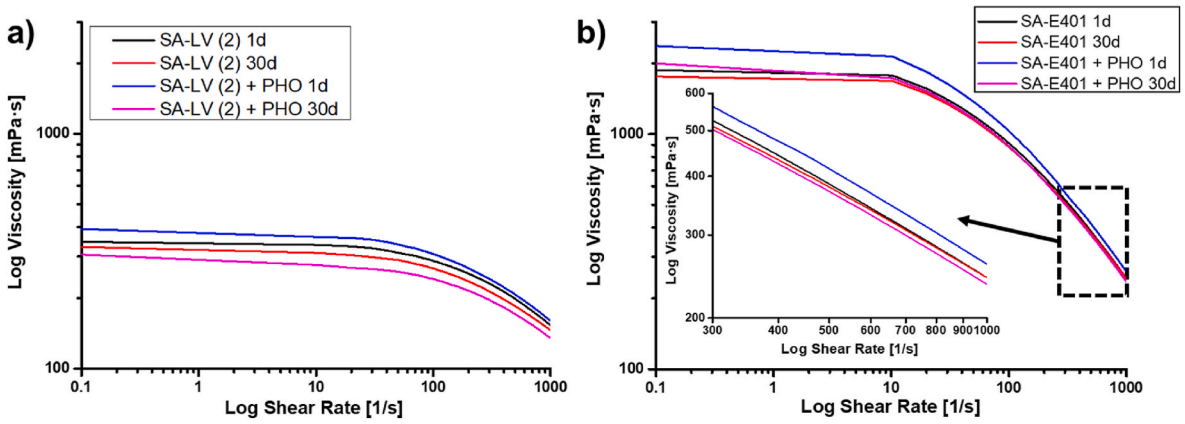

Fig. 5. Log Viscosity *vs.* Log Shear Rate for 2 wt% suspensions of **SA-LV (2) (a)** and **SA-E401 (b)**, pure and supplemented with Eu^{3+}:YPO_4 nanopowders, both freshly prepared (1d) and after 30 days (30d).

viscosity values decreased slightly. With respect to the SA solutions, the suspensions added with phosphors are more viscous when freshly prepared, but less viscous after 30 days. This behaviour could be attributed to an initial stabilization of the suspensions by the phosphors, which diminishes slightly following some settling of the powders. This phenomenon can be attributed to the absence of agitation during the storage period, as the suspensions were not stirred.

3.3. ζ-potential measurements

The prepared solutions of the four different SA grades at 2 wt% concentration were analysed through ζ-potential measurements, both with and without the addition of 0.2 % Eu^{3+}:YPO_4 nanopowders. This analysis was conducted both when the solutions were freshly prepared and after 30 days of ageing, in order to evaluate the stability of the suspensions. The results of this study are presented in Fig. 6, which shows the ζ-potential graphs for all the prepared solutions at different times. Table 2 reports the ζ-average and ζ-deviation values for all the

Table 2
ζ-Potential parameters of freshly prepared and aged SA solutions.

Sample	ζ-Ave (z-Dev) (mV)	
	As-prepared	After 30 days
SA-VLV 2 wt%	−54.9 (11.7)	−33.5 (16.7)
SA-VLV 2 wt% + Eu^{3+}:YPO_4	−63.0 (3.71)	−60.4 (4.13)
SA-LV (1) 2 wt%	−62.7 (4.32)	−55.6 (5.58)
SA-LV (1) 2 wt% + Eu^{3+}:YPO_4	−63.8 (3.99)	−62.3 (3.51)
SA-LV (2) 2 wt%	−56.8 (16.4)	−60.1 (17.9)
SA-LV (2) 2 wt% + Eu^{3+}:YPO_4	−79.0 (4.79)	−77.8 (4.28)
SA-E401 2 wt%	−83.6 (6.95)	−76.7 (7.17)
SA-E401 2 wt% + Eu^{3+}:YPO_4	−94.9 (4.71)	−86.9 (4.48)

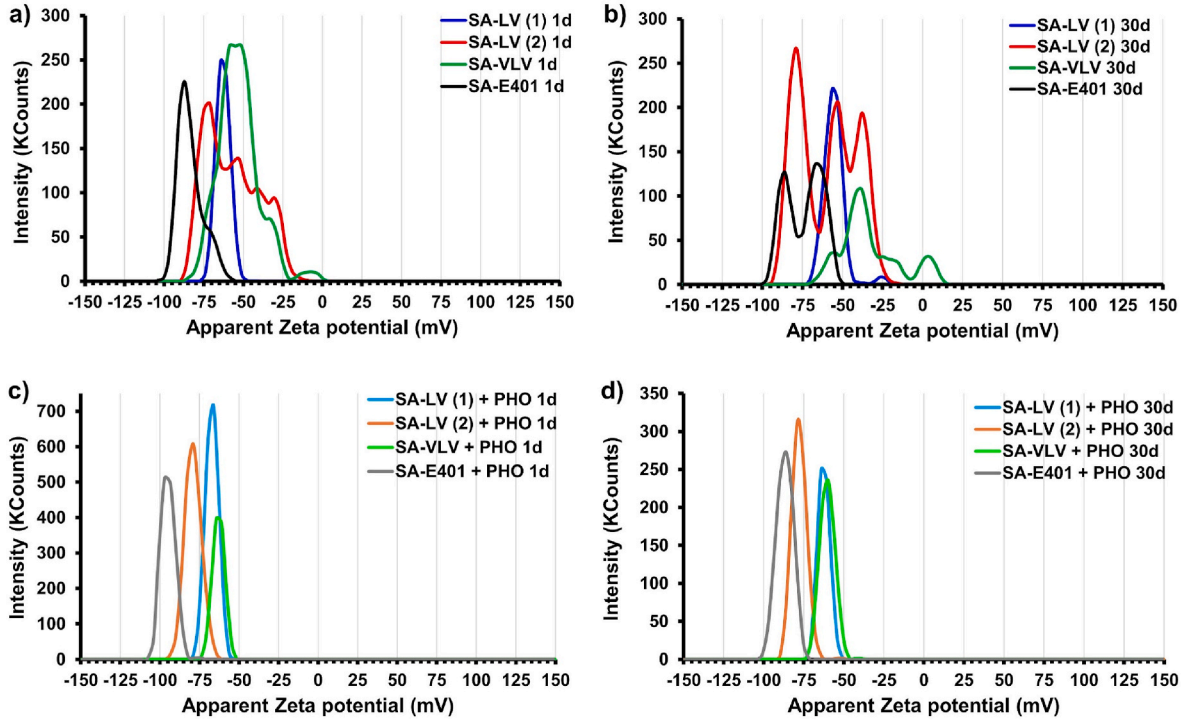

Fig. 6. ζ-Potential measurements on **a)** freshly prepared (1d) SA solutions at 2 wt% conc. **b)** SA solutions at 2 wt% conc. after 30 days of aging (30d). **c)** freshly prepared (1d) SA solutions at 2 wt% conc. with the addition of 0.2 wt% **Eu^{3+}:YPO_4** phosphor nanopowders (10 wt% with respect to SA). **d)** SA solutions at 2 wt% with the addition of 0.2 wt% **Eu^{3+}:YPO_4** phosphor nanopowders (10 wt% with respect to SA) after 30 days of aging (30d).

solutions.

The freshly prepared SA solutions manifest predominantly monomodal peak profiles, with the exception of **SA-LV (2)**, which exhibits a multitude of peaks (Fig. 6(a)). Subsequent to a 30-day period, all solutions exhibited multimodal profiles, with the exception of **SA-LV (1)** (Fig. 6(b)). It is noteworthy that **SA-LV (1)** exhibited turbidity and a trace of precipitate at the base of the vial after 30 days, while the other solutions remained clear.

The results obtained demonstrate the tendency of all SA solutions to form numerous species over time in solution, thereby suggesting a certain degree of instability. It is conceivable that polymeric chains of SA might rearrange in two or more different clusters with different ζ-potentials, or partly decompose, for example through hydrolysis [64]. For specific types of SA (namely **SA-VLV** and **SA-LV (2)**), certain peaks fall below the stability threshold (a suspension is typically deemed stable when $\zeta > |30|$ mV) [65] both in their freshly prepared state and following a 30-day period. The ζ-average potential, however, decreases for all samples after 30 days (see Table 2).

The only exception is **SA-LV (2)**, which exhibits a high level of deviation from the mean. The most unfavourable result overall can be considered that of **SA-VLV**, and the most favourable is that of **SA-E401**. It is evident that pure SA solutions demonstrate a propensity towards instability.

In the case of SA solutions that have been augmented with **Eu^{3+}:YPO_4** nanopowders, monomodal profiles are exhibited in both freshly prepared and 30-day aged states. It is evident that the presence of the nanopowders stabilises all grades of SA, both by preventing the occurrence of multiple peaks and by promoting long-term stability. Furthermore, a more negative net ζ-average value was observed in all cases, both for freshly prepared and aged solutions (see Table 2), indicating an additional stabilization effect compared to pure SA solutions.

It is noteworthy that the water-based suspension of **Eu^{3+}:YPO_4** nanopowders without SA exhibits a negligible negative ζ-potential of -17.5 ± 4.26 mV (see Fig. S3), thus indicating low stability of the suspension. Conversely, this peak is not observed in the analyses of **SA + Eu^{3+}:YPO_4** suspensions. This observation indicates the occurrence of a synergistic interaction between the polymeric dispersant and the phosphor powders. Consequently, it can be concluded that SA stabilises **Eu^{3+}:YPO_4** nanoparticle suspensions, and conversely, the nanophosphor stabilises SA solutions in a mutually beneficial process. Nanoparticles stabilization by SA through shifting ζ-potential to more negative values is known in literature on sepiolite/magnetite [66], metal oxides [67], kaolinite [68] polymeric [69] and gold [65] nanoparticles. Authors of these papers account this stabilization to SA chemisorption to nanoparticles, which expose COO^- and OH groups to the water layer. Electrostatic repulsion of these functional groups attached to SA leads to repulsion of the SA-chemisorbed nanoparticles, leading to higher stabilization. The large difference in ζ-potential values is instead given by SA grades, where SA molecular weight and M/G ratio are the most important factors which determines ζ-potential value: M/G ratio in particular was shown to have higher influence on the negativity of ζ-potential [56].

It is evident that **SA-VLV** and **SA-LV (2)** are the SA grades that most benefit from phosphor stabilization. Without nanophosphors, the aqueous solutions of these two SA grades exhibit multimodal profiles with peaks covering a wide range of ζ-potential. In the case of **SA-VLV**, the average ζ-potential values are particularly low, especially after ageing (see Fig. 6). However, the addition of the nanopowders leads to a significant alteration in the profiles, resulting in monomodal distributions with elevated ζ-potential average values, particularly for **SA-LV (2)**, which emerges as the second-most effective SA after **SA-E401**. The latter is also moderately affected by nanopowders addition, while **SA-LV (1)** is the least sensitive to this treatment (see Table 2).

In conclusion, the inks prepared with **SA-LV (2)** or **SA-E401 + Eu^{3+}:YPO_4** are the most stable. This finding, when combined with the rheology test results, suggests that these two solutions are the most promising for the anti-counterfeiting ink applications and were therefore selected for PL tests.

3.4. Optical properties

The optical behaviour of the alginate-based inks was investigated by photoluminescence (PL) spectroscopy (see Fig. 7).

An excitation wavelength of 280 nm was selected because it activates both the intrinsic emission of the SA matrix and the luminescence of the Eu^{3+}:YPO_4 nanophosphors. To disentangle their respective contributions, PL spectra of pure SA solutions were first recorded.

The phosphorescence properties of sodium alginate are well established [70]. When excited at 280 nm, the main emission lies in the UV region (300–400 nm), but a significant band also extends into the visible range (400–500 nm). This gives sodium alginate (SA) solutions a blue tint under UV light (see Fig. 8). This behaviour originates from chain packing effects and electronic interactions between the carboxylate and hydroxyl groups. These interactions can evolve over time, depending on the composition and polymer conformation [70]. These effects are expected to become even more pronounced when nanoparticles are introduced, as their presence can further influence the organisation of the polymer and, in turn, its photoluminescence response.

To assess the potential effect of shelf life on the optical properties of SA solutions, PL measurements were carried out on freshly prepared solutions and after 30 days. This preliminary test was designed to reveal possible critical changes over time, since the practical use and processability of alginate-based inks could be limited by stability issues. Fig. 7 (a) shows the PL spectrum of a freshly prepared SA-LV(2) solution and after 30 days. The freshly prepared solution exhibits the characteristic emission features of sodium alginate, with a main peak at ~350 nm and additional bands at ~420, 450, and 480 nm [70]. After storage, the relative intensities shift towards the UV contribution, with partial convolution of visible bands, consistent with structural rearrangement and stabilization of the polymer. Importantly, the overall PL intensity remained stable after one month, suggesting no critical loss of performance. A similar trend was observed for the higher-viscosity SA-E401 solution (Fig. 7(b)), where the UV contribution is more dominant due to different chain arrangements in solution. Again, only minor spectral changes occurred over time, while PL intensity was preserved. For clarity, the **insets in** Fig. 7(a) and (b) display the 550–750 nm region, allowing direct comparison of the emission profile of fresh and aged SA solutions.

Fig. 7(c) and (d) report spectra of SA-LV(2) and SA-E401 containing Eu^{3+}:YPO_4 nanoparticles. In these samples, additional emission bands appear above 500 nm, corresponding to the characteristic Eu^{3+} transitions (~600 and ~700 nm) [71]. Although these signals are partly masked by the tail of the much stronger SA emission at ~350 nm, they clearly demonstrate the contribution of Eu^{3+} to the optical response. Notably, after 30 days, both SA–Eu^{3+}:YPO_4 systems showed enhanced visible emission compared to the freshly prepared solutions. This suggests a reorganization of the alginate matrix in the presence of nanoparticles, which modulates both dispersion stability and the photoluminescence response, as also supported by ζ-potential measurements.

Macroscopically, pristine SA solutions display a blue emission under UV light (Fig. 8), whereas Eu^{3+}:YPO_4-loaded inks show a composite color, combining the blue of SA with the characteristic red luminescence of Eu^{3+} (Fig. 9). This dual-emission feature demonstrates the unique properties resulting from the interaction between the matrix and the nanophosphors, confirming the potential of SA–Eu^{3+}:YPO_4 systems for use in anti-counterfeiting applications.

4. Conclusions

In this study, we demonstrated a simple and sustainable strategy to formulate fully water-based luminescent inks by combining Eu^{3+}:YPO_4

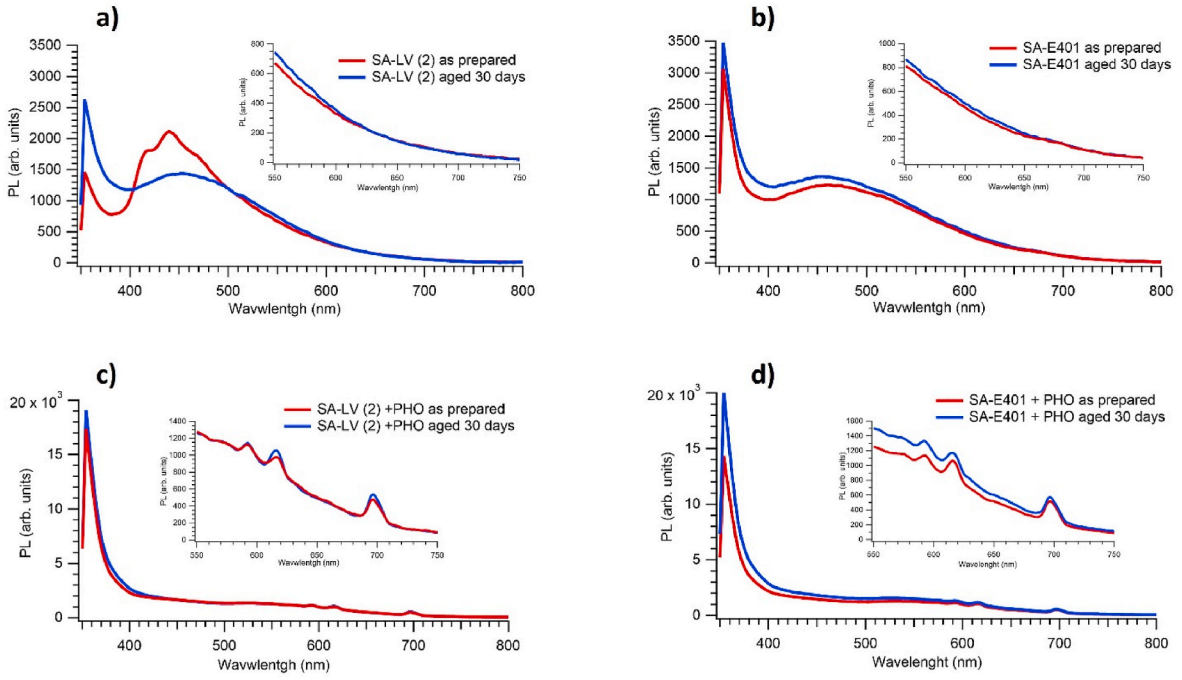

Fig. 7. **(a)** Photoluminescence spectra of **SA-LV(2)** pristine solutions as prepared and after 30 days of aging. **(b)** Photoluminescence spectra of **SA-E401** pristine solutions as prepared and after 30 days of aging. **(c)** Photoluminescence spectra of **SA-LV(2)** + $\mathbf{Eu^{3+}}$**:**$\mathbf{YPO_4}$ suspensions as prepared and after 30 days of aging. **(d)** Photoluminescence spectra of **SA-E401** + $\mathbf{Eu^{3+}}$**:**$\mathbf{YPO_4}$ suspensions as prepared and after 30 days of aging.

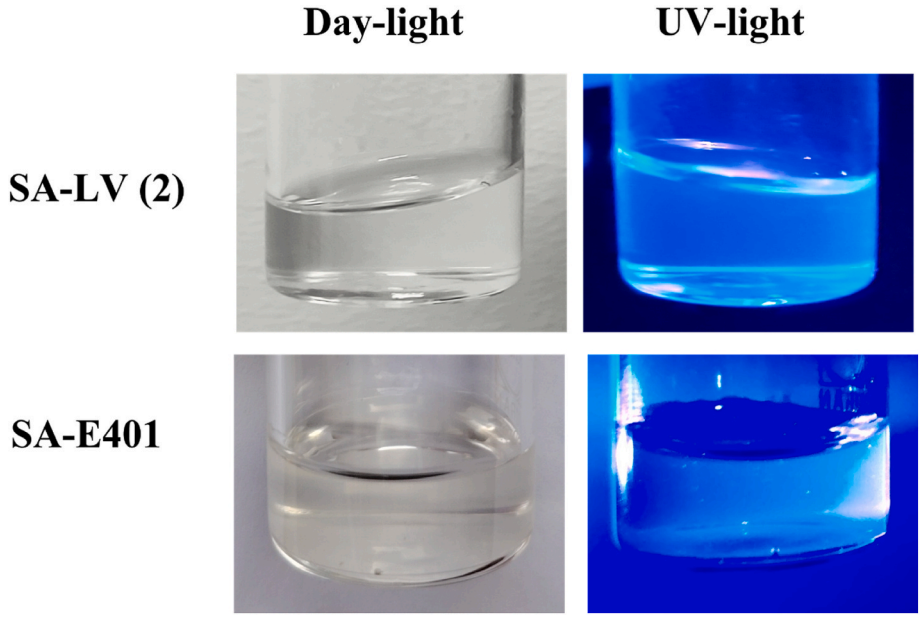

Fig. 8. Digital photos of prepared **SA-LV (2)** 2 wt% and **SA-E401** 2 wt% solutions under irradiation of natural light and UV-light.

nanophosphors with sodium alginate as a dispersant and a rheology modifier.

Stable suspensions with tuneable viscosity were obtained using just three environmentally friendly components, highlighting the effectiveness and environmental compatibility of the approach. Comprehensive rheological, photoluminescence and ζ-Potential analyses revealed strong interactions between the alginate chains and the Eu^{3+}:YPO_4 nanoparticles, which are responsible for both the colloidal stability and the preservation of the optical response of the phosphor. The resulting inks exhibit shear-thinning behaviour, long-term stability, and dual emission from both matrix and nanophosphors, making them promising candidates for anti-counterfeiting and security printing.

Our findings provide a clear proof-of-concept for cost-effective, solvent-free, and fully water-based luminescent inks, thus demonstrating a significant step towards sustainable and practical security inks. Future work will focus on tailoring rheological properties for specific printing technologies and assessing performance in real-world authentication scenarios.

CRediT authorship contribution statement

Enrico Paradisi: Writing – review & editing, Writing – original draft,

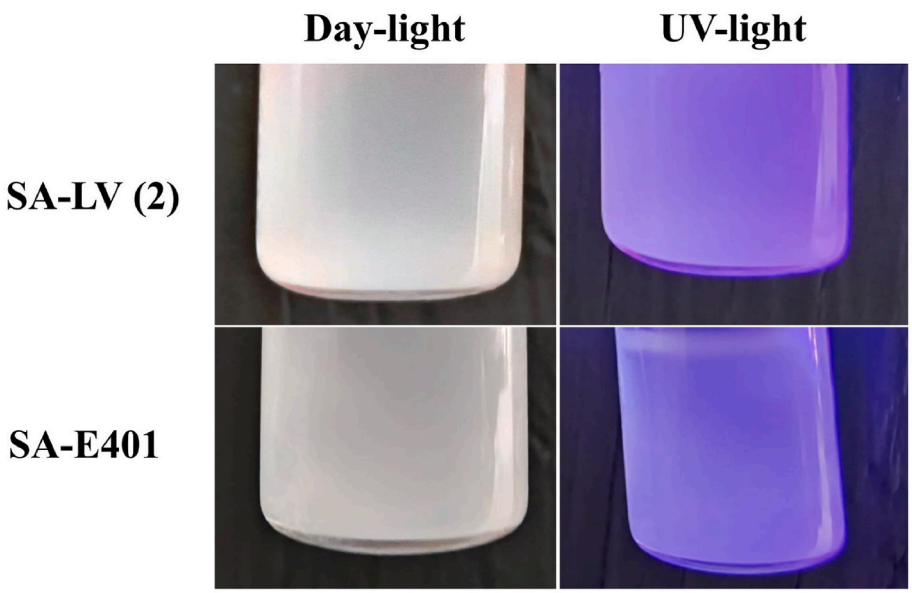

Fig. 9. Digital photos of prepared **SA-LV (2)** 2 wt% + Eu^{3+}:YPO_4 and **SA-E401** 2 wt% + Eu^{3+}:YPO_4 suspensions under irradiation of natural light and UV-light.

Visualization, Validation, Investigation, Data curation, Conceptualization. **Cecilia Mortalò:** Writing – review & editing, Writing – original draft, Validation, Supervision, Methodology, Investigation, Data curation, Conceptualization. **Fernanda Andreola:** Writing – review & editing, Writing – original draft, Investigation. **Valentina Zin:** Writing – review & editing. **Raffaella Capelli:** Writing – original draft, Investigation. **Luca Pasquali:** Writing – original draft, Investigation. **Silvia Maria Deambrosis:** Writing – review & editing. **Enrico Miorin:** Writing – review & editing. **Cristina Leonelli:** Writing – review & editing, Supervision, Resources.

Declaration of competing interest

The authors declare that they have no known competing financial interests or personal relationships that could have appeared to influence the work reported in this paper.

Acknowledgements

No specific grants from public, commercial or non-profit funding bodies were received for this research. C.M. and E.P. would like to thank Dr. Mauro Zapparoli (CIGS - Interdepartmental Centre for Large Instruments, University of Modena and Reggio Emilia) and Monica Montecchi (Department of Engineering “Enzo Ferrari” (DIEF), University of Modena and Reggio Emilia) for their help with the TEM analyses and PL measurements, respectively.

Appendix A. Supplementary data

Supplementary data to this article can be found online at https://doi.org/10.1016/j.ceramint.2025.10.092.

References

[1] M.S. Abdelrahman, T.A. Khattab, Recent advances in photoresponsive printing inks for security encoding applications, Luminescence 39 (6) (2024) e4800, https://doi.org/10.1002/bio.4800.
[2] Y. Wu, W. Wu, Combinations of superior inorganic phosphors for level-tunable information hiding and encoding, Adv. Opt. Mater. 9 (2021) 2100281, https://doi.org/10.1002/adom.202100281.
[3] Pushpendra, B.S. Naidu, Luminescent nanomaterials based covert tags for anticounterfeiting applications: a review, Adv. Colloid Interface Sci. 341 (2025) 103480, https://doi.org/10.1016/j.cis.2025.103480.
[4] W.J. Yao, Q.Y. Tian, W. Wu, Tunable emissions of upconversion fluorescence for security applications, Adv. Opt. Mater. 7 (2019) 1801171, https://doi.org/10.1002/adom.201801171.
[5] T. Luo, G. Jiang, M. Yu, H. Xu, W. Gao, Robust high dynamic range color image watermarking method based on feature map extraction, Signal Process. 155 (2019) 83–95, https://doi.org/10.1016/j.sigpro.2018.09.024.
[6] J. Molina-González, G. Ramírez-García, H. Desirena, O. Meza, Anti-counterfeiting strategy based on multiwavelength photothermal particles to disclose thermal imaging, Ceram. Int. 48 (2022) 9075–9082, https://doi.org/10.1016/j.ceramint.2021.12.091.
[7] M. Wang, B. Duong, H. Fenniri, M. Su, Nanomaterial-based barcodes, Nanoscale 7 (2015) 11240–11247, https://doi.org/10.1039/C5NR01948F.
[8] P. Kumar, S. Singh, B.K. Gupta, Future prospects of luminescent nanomaterials based security ink: from synthesis to anti-counterfeiting applications, Nanoscale 8 (2016) 14297–14340, https://doi.org/10.1039/C5NR06965C.
[9] B.D.D. Cruz, D.M. Correia, R. Polícia, N. Pereira, P. Nunes, M. Fernandes, C. R. Tubio, G. Botelho, S. Lanceros-Méndez, V. de Zea-Bermudez, Photoluminescent alginate-based composite inks for anti-counterfeiting security and soft actuator applications, Chem. Eng. J. 472 (2023) 144813, https://doi.org/10.1016/j.cej.2023.144813.
[10] F. Yan, S. Li, R. Tong, Y. Wang, Y. Fu, L. Chen, Review of phosphorescent carbon dots and their applications, ACS Appl. Nano Mater. 8 (8) (2025) 3709–3725, https://doi.org/10.1021/acsanm.4c06540.
[11] B. Song, H. Wang, Y. Zhong, B. Chu, Y. Su, Y. He, Fluorescent and magnetic anti-counterfeiting realized by biocompatible multifunctional silicon Nanoshuttle-Based security ink, Nanoscale 10 (2018) 1617–1621, https://doi.org/10.1039/C7NR06337G.
[12] W. Luo, G. Wang, Photo-responsive fluorescent materials with aggregation-induced emission characteristics, Adv. Opt. Mater. 8 (2020) 2001362, https://doi.org/10.1002/adom.202001362.
[13] S.A.N. Najafabadi, C. Huang, K. Betlem, T.A. van Voorthuizen, L.C.P.M. de Smet, M.K. Ghatkesar, M. van Dongen, M.A. van der Veen, Advancements in inkjet printing of Metal- and covalent-organic frameworks: process design and ink optimization, ACS Appl. Mater. Interfaces 17 (8) (2025) 11469–11494, https://doi.org/10.1021/acsami.4c15957.
[14] I. Gupta, S. Singh, S. Bhagwan, D. Singh, Rare earth (RE) doped phosphors and their emerging applications: a review, Ceram. Int. 47 (14) (2021) 19282–19303, https://doi.org/10.1016/j.ceramint.2021.03.308.
[15] P. Qiu, N. Zhou, H. Chen, C. Zhang, G. Gao, D. Cui, Recent advances of lanthanide-doped upconversion nanomaterials: synthesis, nanostructures and surface modification, Nanoscale 5 (2013) 11512–11525, https://doi.org/10.1039/C3NR03642A.
[16] S. Chong, B.J. Riley, X. Lu, J. Du, T. Mahadevan, V. Hegde, Synthesis and properties of anhydrous rare-earth phosphates, monazite and xenotime: a review, RSC Adv. 14 (2024) 18978–19000, https://doi.org/10.1039/d4ra01142b.
[17] R.P. Rao, Tb^{3+} activated green phosphors for plasma display panel applications, J. Electrochem. Soc. 150 (8) (2003) H165–H171, https://doi.org/10.1149/1.1583718.
[18] D. Giaume, V. Buissette, K. Lahlil, T. Gacoin, J.-P. Boilot, D. Casanova, E. Beaurepaire, M.-P. Sauviat, A. Alexandrou, Emission properties and applications of nanostructured luminescent oxide nanoparticles, Prog. Solid State Chem. 33 (2005) 99–106, https://doi.org/10.1016/j.progsolidstchem.2005.11.041.
[19] K.C. Barick, A. Sharma, N.G. Shetake, R.S. Ningthoujam, R.K. Vatsa, P.D. Babu, B. N. Pandey, P.A. Hassan, Covalent bridging of surface functionalized Fe_3O_4 and

YPO_4:Eu nanostructures for simultaneous imaging and therapy, Dalton Trans. 44 (2015) 14686–14696, https://doi.org/10.1039/C5DT01522G.
[20] P. Kumar, P.K. Vishwakarma, S.B. Rai, A. Bahadur, Engineered ultra-luminous La/YPO_4:Eu^{3+} nanophosphors for advanced security ink and latent fingerprint (LFPs) detection, J. All. Compd. 1009 (2024) 176827, https://doi.org/10.1016/j.jallcom.2024.176827.
[21] K. Munirathnam, P.C. Nagajyothi, K. Hareesh, M. Madesh Kumar, S.D. Dhole, Effect of Mn codopant on thermoluminescence properties of γ-Rays irradiated $Na_3Y(PO_4)_2$:Dy phosphors for dosimetry applications, Appl. Phys. A 127 (2021) 41, https://doi.org/10.1007/s00339-020-04202-0.
[22] A.K. Soni, K.K. Yadav, B.P. Singh, R. Joshi, S. Chakraborty, R. Chakravarty, N. K. Nagaraja, D.K. Singh, V. Kain, A. Dash, R.S. Ningthoujam, Smart YPO_4:Er−Yb nanophosphor for optical heating, hyperthermia, security ink, cancer endoradiotherapy, and uranyl recovery, ACS Appl. Nano Mater. 4 (2021) 850–860, https://doi.org/10.1021/acsanm.0c03198.
[23] F. Armetta, B. Boiko, D. Hreniak, R.C. Ponterio, M.L. Saladino, Luminescent YPO_4:Eu@PVA dispersions for anti-counterfeiting ink applications, Mater. Lett. 333 (2023) 133653, https://doi.org/10.1016/j.matlet.2022.133653.
[24] B.P. Singh, M. Srivastava, K.V. Ramesh, M.C. Varma, P. Atchutha Rao, B. Sahu, A. Bairagya, S. Devarakonda, H. Korlapati, R.S. Ningthoujam, Nano architectonics of PEGylated YPO_4: Eu^{3+}, Sm^{3+}, Tb^{3+} doped nanoparticles: optical and anticounterfeit applications, Ceram. Int. 51 (2025) 6772–6782, https://doi.org/10.1016/j.ceramint.2024.12.121.
[25] Q. Zhu, Z. Xu, Z. Wang, X. Wang, X. Li, X. Sun, J.-G. Li, Multi-color emission in monodispersed spheres of tetragonal yttrium phosphate: microwave-assisted fast synthesis, formation mechanism, temperature-dependent luminescence, and application in anti-fake labeling, CrystEngComm 20 (2018) 3187–3201, https://doi.org/10.1039/c8ce00365c.
[26] L. Del-Mazo-Barbara, M.-P. Ginebra, Rheological characterisation of ceramic inks for 3D direct ink writing: a review, J. Eur. Ceram. Soc. 41 (2021) 18–33, https://doi.org/10.1016/j.jeurceramsoc.2021.08.031.
[27] X. Chen, Q. Wang, X.J. Wang, J. Li, G.-B. Xu, Synthesis and performance of ZnO quantum dots water-based fluorescent ink for anti-counterfeiting applications, Sci. Rep. 11 (2021) 5841, https://doi.org/10.1038/s41598-021-85468-z.
[28] B. Kalaburgi, B. Daruka Prasad, D.R. Lavanya, S.C. Sharma, C. Srikanth, G. P. Darshan, M. Nasreen Taj, Nagabhushana H. Premkumar, Facile and eco-friendly PVA nanocomposites as a photo-luminescent: anti-counterfeiting, LED and wettability applications, Ceram. Int. 49 (2023) 4586–4598, https://doi.org/10.1016/j.ceramint.2022.09.344.
[29] P. Li, J. Zeng, B. Wang, Z. Cheng, J. Xu, W. Gao, K. Chen, Waterborne fluorescent dual anti-counterfeiting ink based on Yb/Er-carbon quantum dots grafted with dialdehyde nano-fibrillated cellulose, Carbohydr. Polym. 247 (2020) 116721, https://doi.org/10.1016/j.carbpol.2020.116721.
[30] X. Ye, S. Wang, P. Zhou, D. Zhang, P. Zhu, Fluorescent cellulose nanocrystals/waterborne polyurethane nanocomposites for anti-counterfeiting applications, Phys. Chem. Chem. Phys. 25 (2023) 9492, https://doi.org/10.1039/D3CP00654A.
[31] Q. Wang, G. Xu, G. Liu, T. Li, Y. Li, C. Liu, Water-dispersible, fluorescent color-tunable zinc oxide quantum dot preparation for anti-counterfeiting, Ceram. Int. 49 (2023) 13625–13633, https://doi.org/10.1016/j.ceramint.2025.01.206.
[32] S. Liu, J. Wang, F. Tang, N. Wang, L. Li, C. Yao, L. Li, Aqueous systems with tunable fluorescence including white-light emission for anti-counterfeiting fluorescent inks and hydrogels, ACS Appl. Mater. Interfaces 12 (49) (2020) 55269–55277, https://doi.org/10.1021/acsami.0c16815.
[33] J. Xie, X. Sun, X. Guo, X. Feng, K. Chen, X. Shu, C. Wang, W. Sun, Y. Liu, B. Shang, X. Liu, D. Chen, W. Xu, Z. Li, Water-borne, durable and multicolor silicon nanoparticles/sodium alginate inks for anticounterfeiting applications, Carbohydr. Polym. 301 (A) (2023) 120307, https://doi.org/10.1016/j.carbpol.2022.120307.
[34] X. Guo, X. Sun, J. Zhang, Y. Huang, X. Liu, X. Liu, W. Xu, D. Chen, Luminescent mechanism and anti-counterfeiting application of hydrophilic, undoped room-temperature phosphorescent silicon nanocrystals, Small 20 (2024) 2303464, https://doi.org/10.1002/smll.202303464.
[35] J. Li, X. Zhao, X. Gong, Rational design of dual-mode emitting carbon dots to exploit the synergistic effect of matrices for high-efficiency WLEDs and anti-counterfeiting, Adv. Opt. Mater. 12 (2024) 2302297, https://doi.org/10.1002/adom.202302297.
[36] R. Abka-khajouei, L. Tounsi, N. Shahabi, A.K. Patel, S. Abdelkafi, P. Michaud, Structures, properties and applications of alginates, Mar. Drugs 20 (2022) 364, https://doi.org/10.3390/md20060364.
[37] A. Bibi, S. Rehman, A. Yaseen, Alginate-nanoparticles composites: kinds, reactions and applications, Mater. Res. Express 6 (2019) 092001, https://doi.org/10.1088/2053-1591/ab2016.
[38] E. Paradisi, C. Mortalò, P. Russo, V. Zin, E. Miorin, F. Montagner, C. Leonelli, S. M. Deambrois, Facile and effective method for the preparation of sodium Alginate/TiO_2 bio-composite films for different applications, Macromol. Symp. 413 (4) (2024) 2300230, https://doi.org/10.1002/masy.202300230.
[39] B. Kumar, N. Singh, P. Kumar, A review on sources, modification techniques, properties and potential applications of alginate-based modified polymers, Eur. Polym. J. 213 (2024) 113078, https://doi.org/10.1016/j.eurpolymj.2024.113078.
[40] C. Mortalò, P. Russo, E. Miorin, V. Zin, E. Paradisi, C. Leonelli, Extruded composite films based on polylactic acid and sodium alginate, Polymer (2023) 126162, https://doi.org/10.1016/j.polymer.2023.126162.
[41] A. D'Angelo, C. Mortalò, L. Comune, G. Raffaini, M. Fiorentino, M. Catauro, Sol–gel synthesized silica/sodium alginate hybrids: comprehensive physico-chemical and biological characterization, Molecules 30 (2025) 3481, https://doi.org/10.3390/molecules30173481.
[42] A. Dodero, S. Alberti, G. Gaggero, M. Ferretti, R. Botter, S. Vicini, M. Castellano, An up-to-date review on alginate nanoparticles and nanofibers for biomedical and pharmaceutical applications, Adv. Mater. Interfac. 8 (2021) 2100809, https://doi.org/10.1002/admi.202100809.
[43] H. Hecht, S. Srebnik, Structural characterization of sodium alginate and calcium alginate, Biomacromol 17 (2016) 2160–2167, https://doi.org/10.1021/acs.biomac.6b00378.
[44] M.A. Masuelli, C.O. Illanes, Review of the characterization of sodium alginate by intrinsic viscosity measurements. Comparative analysis between conventional and single point methods, Int. J. Biomed. Sci. Eng. 1 (1) (2014) 1–11.
[45] A.T. Mogharbel, G.R.S. Ashour, K. Alkhamis, A.M. Al-bonayan, M.M. Abualnaja, J. Qurban, H.A. Katouah, N.M. El-Metwaly, Preparation of self-healing anthocyanidin-containing thermochromic alginate ink for authentication purposes, ACS Omega 9 (2024) 1562–1572, https://doi.org/10.1021/acsomega.3c07874.
[46] A. Hossan, S.Y. Al nami, Development of photochromic authentication patterns using self-healable sodium alginate hydrogel: optical strategy toward confidential information encryption, Arab. J. Sci. Eng. 49 (2024) 787–800, https://doi.org/10.1007/s13369-023-08488-z.
[47] N. Das, C. Maity, Multi-colored aqueous ink for rewritable paper, Small 20 (2024) 2403512, https://doi.org/10.1002/smll.202403512.
[48] Z. Wang, A. Li, Z. Zhao, T. Zhu, Q. Zhang, Y. Zhang, Y. Tan, W.Z. Yuan, Accessing Excitation- and time-responsive afterglows from aqueous processable amorphous polymer films through doping and energy transfer, Adv. Mater. 34 (2022) 2202182, https://doi.org/10.1002/adma.202202182.
[49] E. Paradisi, C. Mortalò, V. Zin, F. Armetta, V. Boiko, D. Hreniak, M. Zapparoli, S. M. Deambrosis, E. Miorin, C. Leonelli, M.L. Saladino, Eu-Doped YPO_4 luminescent nanopowders for anticounterfeiting applications: tuning morphology and optical properties by a rapid microwave-assisted hydrothermal method, ACS Appl. Nano Mater. 7 (7) (2024) 6893–6905, https://doi.org/10.1021/acsanm.3c05806.
[50] E. Paradisi, C. Mortalò, V. Zin, S.M. Deambrosis, M. Zapparoli, E. Miorin, C. Leonelli, Understanding the effect of temperature on the crystallization of Eu^{3+}:YPO_4 nanophosphors prepared by MW-Assisted method, Ceram. Int. 51 (2025) 7075–7086, https://doi.org/10.1016/j.ceramint.2024.12.144.
[51] V. Riva, D. Boccaccini, M. Cannio, M. Maioli, M. Valle, M. Romagnoli, C. Mortalò, C. Leonelli, Insight into t->m transition of MW treated 3Y-PSZ ceramics by grazing incidence X-ray diffraction, J. Eur. Ceram. Soc. 42 (2022) 227–237, https://doi.org/10.1016/j.jeurceramsoc.2021.09.054.
[52] C. Mortalò, R. Rosa, P. Veronesi, S. Fasolin, V. Zin, S.M. Deambrosis, E. Miorin, G. Dimitrakis, M. Fabrizio, C. Leonelli, Microwave assisted sintering of Na-β''-Al_2O_3 in single mode cavities: insights in the use of 2450 mhz frequency and preliminary experiments at 5800 MHz, Ceram. Int. 46 (2020) 28767–28777, https://doi.org/10.1016/j.ceramint.2020.08.039.
[53] E. Paradisi, R. Rosa, G. Baldi, V. Dami, A. Cioni, G. Lorenzi, C. Leonelli, Microwave–assisted vacuum synthesis of TiO_2 nanocrystalline powders in one–pot, one–step procedure, Nanomaterials 12 (2022) 149, https://doi.org/10.3390/nano12010149.
[54] P. Parhi, V. Manivannan, Novel Microwave Initiated Solid-State Metathesis Synthesis and Characterization of Lanthanide Phosphates and Vanadates, LMO_4 (L=Y, La and M=V, P), Solid State Sci. 10 (2008) 1012–1019, https://doi.org/10.1016/j.solidstatesciences.2007.11.038.
[55] P.R. de Souza Mendes, R.L. Thompson, Time-dependent yield stress materials, Curr. Opin. Colloid Interface Sci. 43 (2019) 15–25, https://doi.org/10.1016/j.cocis.2019.01.018.
[56] A. Dodero, I. Donati, S. Scarfì, S. Mirata, S. Alberti, P. Lova, D. Comoretto, M. Alloisio, S. Vicini, M. Castellano, Effect of sodium alginate molecular structure on electrospun membrane cell adhesion, Mater. Sci. Eng. C 124 (2021) 112067, https://doi.org/10.1016/j.msec.2021.112067.
[57] Q. Xu, L. Sun, B. Zhang, J. Li, J. Gao, C. Nie, X. Shi, S. Sun, B. Teng, Y. Zhang, D. Zhong, Crystal growth and spectroscopic performances of Dy^{3+}:YPO_4 and Dy^{3+}/Tb^{3+}:YPO_4 crystal as potential yellow laser gain mediums, J. Alloys Compd. 996 (2024) 174855, https://doi.org/10.1016/j.jallcom.2024.174855.
[58] F. Armetta, V. Boiko, D. Hreniak, C. Mortalò, C. Leonelli, L. Barbata, M.L. Saladino, Effect of the hydrothermal time on the forming specific morphology of YPO_4:Eu^{3+} nanoparticles for dedicated luminescent applications as optical markers, Ceram. Int. 49 (2023) 23287–23294, https://doi.org/10.1016/j.ceramint.2023.04.159.
[59] H. Barnes, A Handbook of Elementary Rheology, University of Wales, 2000. ISBN: 0-9538032-0-1.
[60] S. Fu, A. Thacker, D.M. Sperger, R.L. Boni, S. Velankar, E.J. Munson, L.H. Block, Rheological evaluation of inter-grade and inter-batch variability of sodium alginate, AAPS PharmSciTech 11 (4) (2010) 1662–1674, https://doi.org/10.1208/s12249-010-9547-0.
[61] F. Belalia, N.-E. Djelali, Rheological properties of sodium alginate solutions, Rev. Roum. Chem. 59 (2) (2014) 135–145.
[62] C. Rodríguez-Rivero, L. Hilliou, E.M. Martín del Valle, et al., Rheological characterization of commercial highly viscous alginate solutions in shear and extensional flows, Rheol. Acta 53 (2014) 559–570, https://doi.org/10.1007/s00397-014-0780-4.
[63] B. Maciel, C. Oelschlaeger, N. Willenbacher, Chain flexibility and dynamics of alginate solutions in different solvents, Colloid Polym. Sci. 298 (2020) 791–801, https://doi.org/10.1007/s00396-020-04612-9.
[64] M.S. Shoichet, R.H. Li, M.L. White, S.R. Winn, Stability of hydrogels used in cell encapsulation: an *in vitro* comparison of alginate and agarose, Biotechnol. Bioeng. 50 (1996) 374–381, https://doi.org/10.1002/(SICI)1097-0290(19960520)50:4<374::AID-BIT4>3.0.CO, 2-I.
[65] H. Liu, K. Ikeda, M.T. Nguyen, S. Sato, N. Matsuda, H. Tsukamoto, T. Tokunaga, T. Yonezawa, Alginate-stabilized gold nanoparticles prepared using the

microwave-induced plasma-in-liquid process with long-term storage stability for potential biomedical applications, ACS Omega 7 (2022) 6238–6247, https://doi.org/10.1021/acsomega.1c06769.

[66] M.M. Abrougui, M.T. Lopez-Lopez, J.D.G. Duran, Mechanical properties of magnetic gels containing rod-like composite particles, Phil. Trans. R. Soc. A 377 (2019) 20180218, https://doi.org/10.1098/rsta.2018.0218.

[67] V. Slabov, G. Jain, I. Chernyshova, H. Rao Kota, H. Ertesvåg, Alginates as green flocculants for metal oxide nanoparticles, Trans. Indian Inst. Met. 77 (12) (2024) 4169–4179, https://doi.org/10.1007/s12666-023-02957-7.

[68] X. Wei, X. Mao, W. Qin, H. Zeng, J. Han, Synthesis of a green ALG@KLN adsorbent for high-efficient recovery of rare Earth elements from aqueous solution, Sep. Purif. Technol. 325 (2023) 124690, https://doi.org/10.1016/j.seppur.2023.124690.

[69] N. Rescignano, E. Fortunati, I. Armentano, R. Hernandez, C. Mijangos, R. Pasquino, J.M. Kenny, Use of alginate, chitosan and cellulose nanocrystals as emulsion stabilizers in the synthesis of biodegradable polymeric nanoparticles, J. Colloid Interface Sci. 445 (2015) 31–39, https://doi.org/10.1016/j.jcis.2014.12.032.

[70] X. Dou, Q. Zhou, X. Chen, Y. Tan, X. He, P. Lu, K. Sui, B.Z. Tang, Y. Zhang, W. Z. Yuan, Clustering-triggered emission and persistent room temperature phosphorescence of sodium alginate, Biomacromol 19 (6) (2018) 2014–2022, https://doi.org/10.1021/acs.biomac.8b00123.

[71] S. Majeed, M. Bashir, S.A. Shivashankar, Dispersible crystalline nanobundles of YPO_4 and Ln (Eu, Tb)-Doped YPO_4: rapid synthesis, optical properties and bio-probe applications, J. Nanopart. Res. 17 (2015) 309, https://doi.org/10.1007/s11051-015-3113-3.